



Cite this: *Soft Matter*, 2015, 11, 7428

Received 21st April 2015,
Accepted 5th August 2015

DOI: 10.1039/c5sm00943j

www.rsc.org/softmatter

An island of stability in a sea of fingers: emergent global features of the viscous-flow instability†

Irmgard Bischofberger,* Radha Ramachandran and Sidney R. Nagel

The displacement of a more viscous fluid by a less viscous one in a quasi-two dimensional geometry leads to the formation of complex fingering patterns. This fingering has been characterized by a most unstable wavelength, λ_c , which depends on the viscosity difference between two immiscible fluids and sets the characteristic width of the fingers. How the finger length grows after the instability occurs is an equally important, but previously overlooked, aspect that characterizes the global features of the patterns. Long after the instability onset, once the fingers are growing in a nearly steady-state regime, there is a stable inner region where the outer fluid is completely displaced. We show that the ratio of the finger length to the radius of this stable region depends only on the viscosity ratio of the fluids and is decoupled from λ_c .

1 Introduction

One of the earliest and most important examples of pattern formation is the viscous-fingering instability, which occurs when a less viscous fluid displaces a more viscous one confined within a thin gap. Since the work of Saffman and Taylor in 1958,¹ a large amount of literature has been dedicated to interpreting the formation of these structures.^{2–17} Understanding their evolution is important not only for the science of pattern formation,^{18–20} but also for industrial applications ranging from hydrology and petroleum extraction to sugar refining and carbon sequestration.^{21–24}

The majority of this work has been focused on understanding the onset of the instability, when a circular interface develops small finger-like protrusions.^{7,8,10,14–16,25,26} These studies are typically done in a Hele-Shaw cell, which consists of two parallel plates separated by a thin gap, where a high viscosity fluid, η_{out} , is displaced by a lower viscosity fluid, η_{in} . Saffman and Taylor showed that there is a most unstable wavelength, λ_c , that depends on the difference in viscosity, $\Delta\eta \equiv \eta_{\text{out}} - \eta_{\text{in}}$, the interfacial tension, σ , the interfacial velocity, V , and the plate separation, b :¹

$$\lambda_c = \pi b \sqrt{\frac{\sigma}{\Delta\eta V}} \quad (1)$$

This equation describes the experimentally observed selected wavelength reasonably well at lower capillary numbers $Ca = \Delta\eta V/\sigma$,

The James Franck and Enrico Fermi Institutes and The Department of Physics, The University of Chicago, Chicago, Illinois 60637, USA.

E-mail: ibischofberger@uchicago.edu; Tel: +1 773 702 7204

† Electronic supplementary information (ESI) available: Movies of the viscous fingering instability for two different viscosity ratios: $\eta_{\text{in}}/\eta_{\text{out}} = 0.0033$ and $\eta_{\text{in}}/\eta_{\text{out}} = 0.42$. See DOI: 10.1039/c5sm00943j

while deviations occur at larger Ca which have been carefully addressed in a number of recent studies.^{14–16}

However, by focusing on the wavelength selection at the instability onset, previous studies neglect the global features of the fingering patterns that are formed at later times after the fingers are fully developed. We find that these patterns are characterized not only by the finger width, but also by their length. In particular, we find an interior region in which the outer fluid is completely displaced. This provides a scale to measure the finger length as the growth proceeds. This is shown in the three images of Fig. 1. In all cases, the viscosity difference, $\Delta\eta$, the interfacial tension, σ , the plate spacing, b , and the flow rate, q , are held nearly constant as given in the figure caption. The distinctively different patterns are created simply by varying the viscosity ratio, $\eta_{\text{in}}/\eta_{\text{out}}$. With increasing $\eta_{\text{in}}/\eta_{\text{out}}$, the inner

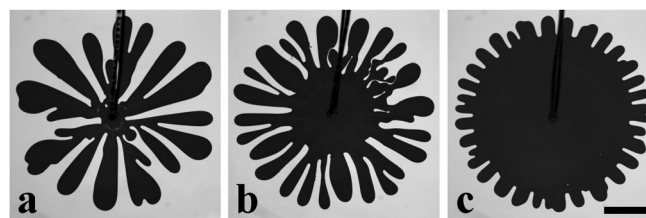


Fig. 1 Fingering patterns showing the presence of an inner circular region of complete displacement of the outer fluid. The inner circle increases with increasing viscosity ratio of the inner to the outer fluid, $\eta_{\text{in}}/\eta_{\text{out}}$, while the most unstable wavelength, λ_c , is approximately held constant. (a) $\eta_{\text{in}}/\eta_{\text{out}} = 0.0033$ ($\eta_{\text{out}} = 296.7$ mPa s, $\eta_{\text{in}} = 0.99$ mPa s), (b) $\eta_{\text{in}}/\eta_{\text{out}} = 0.14$ ($\eta_{\text{out}} = 345.1$ mPa s, $\eta_{\text{in}} = 46.6$ mPa s) and (c) $\eta_{\text{in}}/\eta_{\text{out}} = 0.42$ ($\eta_{\text{out}} = 530.3$ mPa s, $\eta_{\text{in}} = 224.4$ mPa s). In all cases, the colorless outer fluid is a silicone oil and the dyed inner fluid is a glycerol–water mixture. In these experiments, $\Delta\eta = 300 \pm 6$ mPa s, $b = 254$ μm , $q = 10$ ml min^{-1} and $\sigma = 26.5 \pm 2.5$ mN m^{-1} . The scale bar is 4 cm.

circular region increases dramatically while the length of the fingers compared to the inner radius decreases.

While such behavior was previously noted in the specific singular case of miscible fluids where the interfacial tension is nearly zero,²⁷ we show here that this is a much more general result that applies even for immiscible fluids. In particular, by working with immiscible fluids, we demonstrate that the inner region is independent of all the parameters that control the most unstable wavelength. This could not be done in experiments with miscible fluids where λ_c in eqn (1) is cut off by the plate spacing, b .^{14–16,26,28} The finger length is thus set separately from the finger width and is independent of the types of fluids used. It is a general feature of fingering patterns after the non-linear growth has entered into a nearly steady-state regime. This discovery opens up new ways to control the instability.

2 Experimental

The experimental set-up consists of two glass plates of 14 cm radius and 1.9 cm thickness to form the Hele-Shaw cell. The plates are maintained at a constant gap, b , by placing spacers of various thicknesses, ranging from 177 μm to 635 μm , at the edges of the plates. The liquids are injected through a 1.6 mm hole in the center of the plate using a syringe pump (New Era Pump Systems NE-1010) that maintains the volumetric flow rate at a set constant value. The patterns are recorded at frame rates ranging from 2 fps to 14 fps.

In our experiments, we use silicone oils (Clearco) of viscosities ranging between 98 mPa s and 1025 mPa s as the outer fluid. Both glycerol–water mixtures (Fisher Scientific) and mineral oils

(Fisher Scientific) are used as the inner fluids. These two combinations have very different interfacial tensions: 24–29 mN m^{-1} for pairs of silicone oil/glycerol–water mixtures and 1–1.2 mN m^{-1} for pairs of silicone oil/mineral oil combinations. The inner fluids are dyed using Brilliant Blue G dye (Alfa Aesar) or Oil Red O dye (Sigma-Aldrich) to enhance the contrast between the inner and outer fluids. Interfacial tensions, measured using the pendant drop method, are in agreement with literature values.²⁹ Viscosities of all fluids are measured using glass capillary viscometers (Cannon-Fenske). Advancing and receding contact angles, θ_{adv} and θ_{rec} , are measured on the glass plates used in the experiments; silicone oil: $\theta_{\text{adv/rec}} = 0^\circ$, and glycerol–water mixture: $\theta_{\text{adv}} = 59^\circ$ and $\theta_{\text{rec}} = 14^\circ$.

To characterize the overall shape of the patterns, we define three characteristic length scales as shown in the top panel of Fig. 2. We define an inner radius, R_i , which is the radius of the largest circle that fits completely inside the inner fluid and an outer radius, R_o , which is the smallest circle that encloses the entire pattern. The length of the finger is $R_f \equiv R_o - R_i$. The size ratio $\equiv R_f/R_i$.

The most unstable wavelength, λ_c , is determined by half the width of a finger before a splitting event, as shown in the

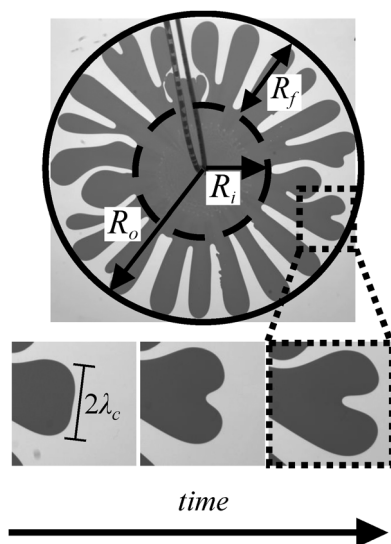


Fig. 2 Determination of the characteristic length scales defining the large-scale structure and the most unstable wavelength, λ_c . The inner radius, R_i , is the radius of the largest circle completely inscribed in the inner fluid. The outer radius, R_o , is the radius of the smallest circle that encloses the entire pattern. The finger length is $R_f \equiv R_o - R_i$. λ_c is defined as half the width of a finger just before it splits, as indicated in the time series of three images in the bottom panel.

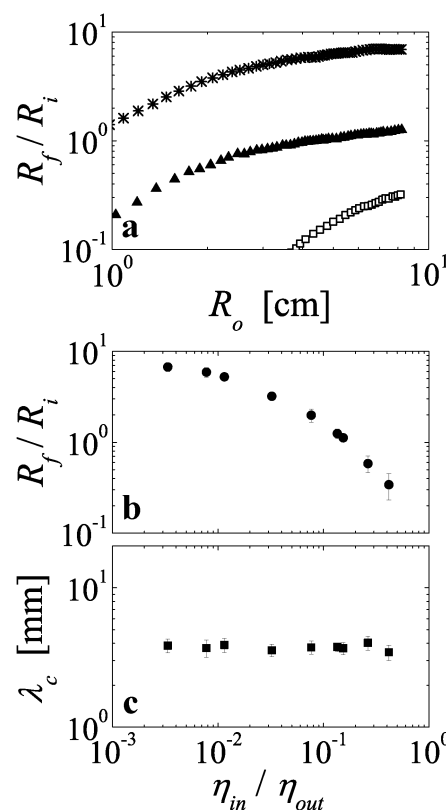


Fig. 3 (a) Growth of the size ratio, R_f/R_i , with the outer radius, R_o , for three different viscosity ratios: (*) $\eta_{\text{in}}/\eta_{\text{out}} = 0.0033$ ($\eta_{\text{out}} = 296.7$ mPa s, $\eta_{\text{in}} = 0.99$ mPa s), (\blacktriangle) $\eta_{\text{in}}/\eta_{\text{out}} = 0.14$ ($\eta_{\text{out}} = 345.1$ mPa s, $\eta_{\text{in}} = 46.6$ mPa s), and (\square) $\eta_{\text{in}}/\eta_{\text{out}} = 0.42$ ($\eta_{\text{out}} = 530.3$ mPa s, $\eta_{\text{in}} = 224.4$ mPa s). (b) and (c) The dependence of the size ratio, R_f/R_i , and the most unstable wavelength, λ_c , on $\eta_{\text{in}}/\eta_{\text{out}}$. The size ratio is measured at $R_o = 8$ cm. In these experiments, $\Delta\eta$ is approximately constant ($\Delta\eta = 300 \pm 6$ mPa s) and $b = 254$ μm , $q = 10$ ml min^{-1} , and $\sigma = 26.5 \pm 2.5$ mN m^{-1} . R_f/R_i changes dramatically with viscosity ratio, while λ_c is unchanged.

bottom panels of Fig. 2. To account for the decrease in velocity with the distance from the center of our radial cell, we only consider splitting events that occur within a radius of 3 cm to 5 cm from the nozzle.

3 Results and discussion

The growth of the patterns is characterized by an initial fast growth of R_f/R_i that gradually slows down as the pattern grows larger, as shown in Fig. 3a for three different viscosity ratios. While the overall dependence is similar for all three datasets, the absolute value of R_f/R_i is very different, indicating that the circular region grows by different amounts (see Movies, ESI†). We focus here on the temporal evolution of the inner radius, R_i , which continues in the steady-state regime long after the onset of fingering.

We note that the radial geometry is known to produce a small delay in the onset of the instability which can also lead to the appearance of a circular stable region. However, this effect is very small for our experiments; this onset radius corresponds to approximately 1.5 mm (comparable to the central injection hole in our plates).^{7,11} It thus does not explain the large central stable region we observe.

To compare the patterns formed at different viscosity ratios, we measure R_f/R_i when the outer radius R_o reaches 8 cm.

In Fig. 3b we show that R_f/R_i measured at this value decreases rapidly with increasing η_{in}/η_{out} . As η_{in}/η_{out} approaches 1, the system goes towards a completely stable displacement. In the other limiting case, when η_{in}/η_{out} approaches 0, the patterns have a vanishingly small inner stable region. In all of these data, we have varied η_{in}/η_{out} in such a way as to leave $\Delta\eta$ nearly constant ($\Delta\eta = 300 \pm 6$ mPa s). We have also kept q , b and σ the same. As shown in Fig. 3c, the most unstable wavelength does not change under these conditions, whereas R_f/R_i drops by more than a decade and a half.

R_f/R_i clearly depends on the viscosity ratio, η_{in}/η_{out} . To understand on what other parameters it might depend, we systematically vary one of the control parameters at a time, while leaving the others fixed. The results are shown in Fig. 4. In the left-most column, we show that a change in $\Delta\eta$ by a decade leaves R_f/R_i unchanged. The most unstable wavelength, however, decreases with increasing $\Delta\eta$ consistent with eqn (1). In the middle and right columns, we show similar behavior when we vary the plate spacing, b , and the flow rate, q . In all cases, R_f/R_i remains unchanged while the most unstable wavelength continues to vary in agreement with the Saffman–Taylor prediction, as indicated by the solid lines in Fig. 4b, d and f which correspond to eqn (1). It is important to note that our experiments are performed within the range of capillary numbers, Ca, where eqn (1) and recent improved theories almost coincide.^{13–16} A comparison with eqn (1) is therefore justified.

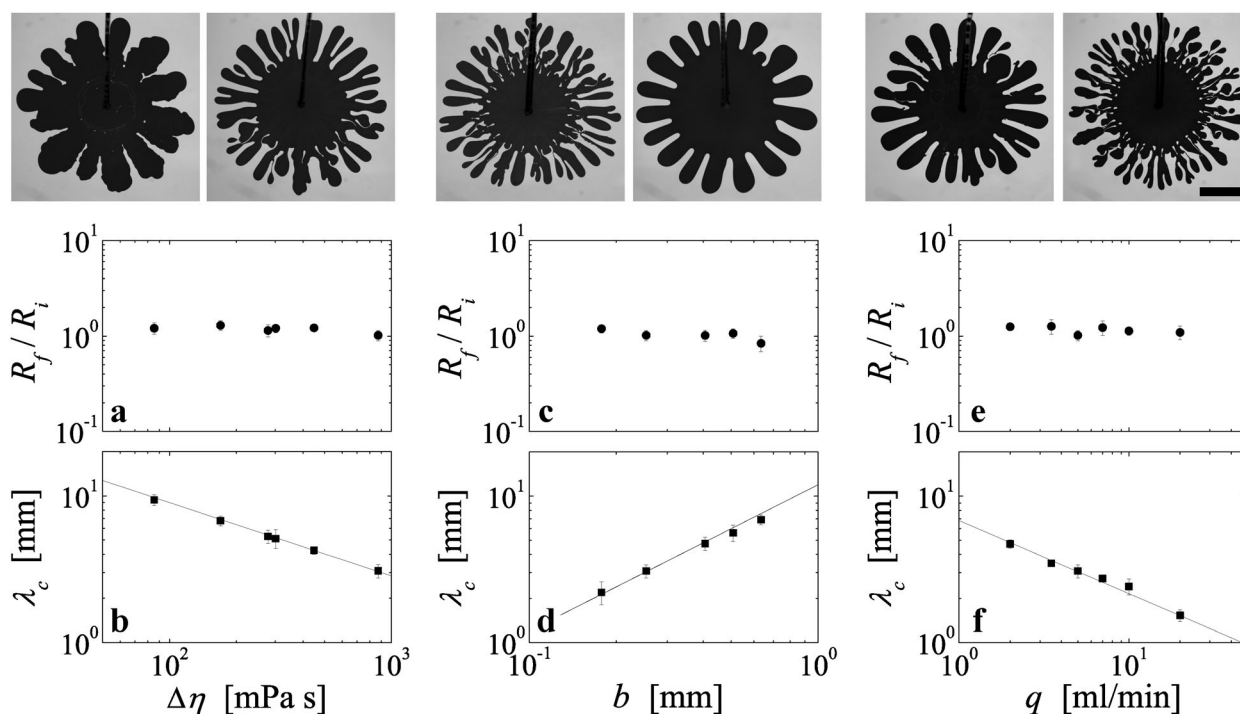


Fig. 4 Dependence of the size ratio, R_f/R_i , and the most unstable wavelength, λ_c , on the viscosity difference, $\Delta\eta$, plate spacing, b , and flow rate, q . The three control parameters are changed one at a time, while keeping the others constant. (a and b) $\eta_{in}/\eta_{out} = 0.15$; $\Delta\eta$ is varied while keeping $q = 5$ ml min⁻¹, $b = 254$ μ m and $\sigma = 26.5 \pm 2.5$ mN m⁻¹. (c and d) $\eta_{in}/\eta_{out} = 0.15$; b is varied while keeping $\Delta\eta = 871.8$ mPa s, $q/b = 196.9$ sq cm min⁻¹, and $\sigma = 26.5 \pm 2.5$ mN m⁻¹. (e and f) $\eta_{in}/\eta_{out} = 0.15$; q is varied while keeping $\Delta\eta = 871.8$ mPa s, $b = 254$ μ m, and $\sigma = 26.5 \pm 2.5$ mN m⁻¹. The lines in (b, d and f) denote the predicted wavelengths according to eqn (1). In all cases, R_f/R_i is unaffected while λ_c varies in accord with eqn (1). The size ratio is measured at $R_o = 8$ cm. The scale bar is 4 cm.

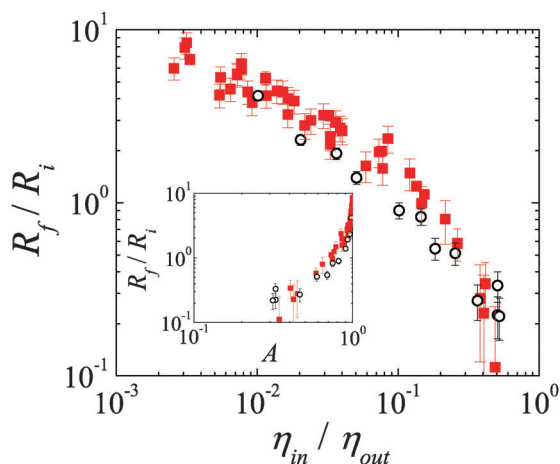


Fig. 5 Dependence of the size ratio, R_f/R_i , on the viscosity ratio, η_{in}/η_{out} , for two sets of fluids with different interfacial tensions, σ . The red squares denote pairs of silicone oil/glycerol–water mixture with $\sigma = 24\text{--}29\text{ mN m}^{-1}$, and the black open circles denote pairs of silicone oil/mineral oil with $\sigma = 1\text{--}1.2\text{ mN m}^{-1}$. The size ratio is measured at $R_o = 8\text{ cm}$. The two datasets are nearly the same, even though the interfacial tensions differ by a factor of approximately 25. Inset: The same R_f/R_i data plotted versus $A \equiv (\eta_{out} - \eta_{in})/(\eta_{out} + \eta_{in})$.

The agreement between eqn (1) and our experimental data further implies that the wavelength selection at tip-splitting events in the non-linear regime follows the same dependencies as that governing the instability onset in the linear regime. The main focus here, however, is on the novel aspect of the pattern growth in the non-linear regime given by R_f/R_i , which is independent of the wavelength selection and therefore the tip-splitting events. The images at the top of each column in Fig. 4 show the patterns at the two extreme values of $\Delta\eta$, b and q ; it is strikingly obvious that they have nearly constant inner radii but very different finger widths.

Fig. 5 shows the dependence of the size ratio on the viscosity ratio for two sets of fluids, glycerol–water mixtures/silicone oils and mineral oils/silicone oils. These fluids have interfacial tensions that differ by approximately a factor of 25. The two datasets are essentially indistinguishable, indicating that R_f/R_i is independent of σ and only controlled by η_{in}/η_{out} . We further tested the influence of the wetting properties of the fluids on the pattern formation by either injecting glycerol–water mixtures into silicone oil or by reversing the order and injecting silicone oil into glycerol–water mixtures. The two liquids have different wetting properties; silicone oil fully wets the glass while glycerol–water mixtures only partially wet glass. The patterns formed in the two sets of experiments are essentially indistinguishable, both in terms of the dependence of R_f/R_i on η_{in}/η_{out} and in terms of λ_c , indicating that the wetting properties do not affect the pattern growth. Lastly, we note that the patterns are further independent of the size of the Hele-Shaw cell; patterns formed in a cell of 25 cm radius are indistinguishable from those formed in a cell of 14 cm radius.

The inset of Fig. 5 shows the same data for R_f/R_i plotted versus $A \equiv (\eta_{out} - \eta_{in})/(\eta_{out} + \eta_{in})$, a quantity that is also just a function of η_{in}/η_{out} and that is sometimes used as a dimensionless

parameter.^{2,30,31} As A approaches 1, R_f/R_i increases rapidly within a very small range of A . Thus plotting R_f/R_i versus η_{in}/η_{out} instead of A allows the global features of the instability to be seen more clearly.

The importance of η_{in}/η_{out} in governing the growth of R_o and R_i emerges from a simple analysis of the pressure drops in the two fluids after the instability has been fully established.²⁷ It was shown in the case of miscible fluids that the interface at R_o and the interface at R_i indeed move at different velocities depending on η_{in}/η_{out} . This analysis can be extended to immiscible fluids where there is an extra contribution to the pressure due to the presence of interfacial tension. However, a more quantitative analysis of the growth requires knowledge of the profile of the pressure contour lines in front of R_o and behind R_i . Such studies are currently underway.

Taken together, the data in Fig. 3–5 show that while the most unstable wavelength is indeed well described by eqn (1), there is a second parameter that characterizes the large-scale features of the patterns. This second parameter, R_f/R_i , is completely independent of the most unstable wavelength, λ_c . It is only set by the viscosity ratio, η_{in}/η_{out} .

4 Conclusions

Looking at the images presented in this paper, three features immediately pop out and grab our attention. First is the presence of fingers that have characteristic widths given by the most unstable wavelength, λ_c . This feature has been studied thoroughly both experimentally and theoretically. Equally apparent, but hitherto neglected, is the presence of a large circular region where the outer fluid is completely displaced. Finally, we see a large variation in the length of the fingers. Our data show that the finger length is unrelated to the finger width and is set by only two parameters: the viscosity ratio, η_{in}/η_{out} , and the radius of the inner circular region.

The experiments presented here show that this result is very general; it applies not only to miscible fluids²⁷ (where interfacial tension approaches zero and singular effects could be important^{32–34}) but also to immiscible pairs of fluids where we are able to vary λ_c . We have thus shown that the two most prominent features of the global patterns, the finger width and length, are independent of one another. While the present experiments have been conducted in a radial Hele-Shaw cell, it is important to see if the large-scale features found here are also present in a linear geometry.

Acknowledgements

We thank Rudro Rana Biswas, Justin Burton, Todd Dupont, Julian Freed-Brown, Leo Kadanoff, Paul Wiegmann, Tom Witten and Wendy Zhang. This work was supported by NSF grant DMR-1404841. I.B. gratefully acknowledges financial support from the Swiss National Science Foundation (PBF2-134287).

References

- 1 P. G. Saffman and G. Taylor, *Proc. R. Soc. A*, 1958, **245**, 312–329.
- 2 G. M. Homsy, *Annu. Rev. Fluid Mech.*, 1987, **19**, 271–311.
- 3 L. Paterson, *J. Fluid Mech.*, 1981, **113**, 513–529.
- 4 J.-D. Chen, *Exp. Fluids*, 1987, **5**, 363–371.
- 5 K. J. Måløy, J. Feder and T. Jøssang, *Phys. Rev. Lett.*, 1985, **55**, 2688.
- 6 D. Bensimon, L. P. Kadanoff, S. Liang, B. I. Shraiman and C. Tang, *Rev. Mod. Phys.*, 1986, **58**, 977.
- 7 J. Miranda and M. Widom, *Phys. D*, 1998, **120**, 315–328.
- 8 M. G. Moore, A. Juel, J. M. Burgess, W. McCormick and H. L. Swinney, *Phys. Rev. E: Stat., Nonlinear, Soft Matter Phys.*, 2002, **65**, 030601.
- 9 O. Praud and H. L. Swinney, *Phys. Rev. E: Stat., Nonlinear, Soft Matter Phys.*, 2005, **72**, 011406.
- 10 N. Goyal and E. Meiburg, *J. Fluid Mech.*, 2006, **558**, 329–355.
- 11 T. T. Al-Housseiny, P. A. Tsai and H. A. Stone, *Nat. Phys.*, 2012, **8**, 747–750.
- 12 L. Cueto-Felgueroso and R. Juanes, *J. Fluid Mech.*, 2014, **758**, 522–552.
- 13 T. Maxworthy, *Phys. Rev. A: At., Mol., Opt. Phys.*, 1989, **39**, 5863.
- 14 H. Kim, T. Funada, D. D. Joseph and G. Homsy, *Phys. Fluids*, 2009, **21**, 074106.
- 15 E. O. Dias and J. A. Miranda, *Phys. Rev. E: Stat., Nonlinear, Soft Matter Phys.*, 2013, **88**, 013016.
- 16 M. Nagel and F. Gallaire, *Phys. Fluids*, 2013, **25**, 124107.
- 17 S. A. Setu, I. Zacharoudiou, G. J. Davies, D. Bartolo, S. Moulinet, A. A. Louis, J. M. Yeomans and D. G. Aarts, *Soft Matter*, 2013, **9**, 10599–10605.
- 18 Y. Couder, *Perspect. Fluid Dyn.*, 2002, **2**, 3.
- 19 G. Daccord, J. Nittmann and H. E. Stanley, *Phys. Rev. Lett.*, 1986, **56**, 336.
- 20 J. Casademunt, *Chaos*, 2004, **14**, 809–824.
- 21 S. Hill, *et al.*, *Chem. Eng. Sci.*, 1952, **1**, 247–253.
- 22 F. Orr and J. Taber, *Science*, 1984, **224**, 563–569.
- 23 A. R. White and T. Ward, *Chaos*, 2012, **22**, 037114.
- 24 Z. Wang, W. A. Jury, A. Tuli and D.-J. Kim, *Vadose Zone J.*, 2004, **3**, 549–559.
- 25 P. Tabeling, G. Zocchi and A. Libchaber, *J. Fluid Mech.*, 1987, **177**, 67–82.
- 26 E. Lajeunesse, J. Martin, N. Rakotomalala and D. Salin, *Phys. Rev. Lett.*, 1997, **79**, 5254.
- 27 I. Bischofberger, R. Ramachandran and S. R. Nagel, *Nat. Commun.*, 2014, **5**, 5265.
- 28 L. Paterson, *Phys. Fluids*, 1985, **28**, 26–30.
- 29 P. Than, L. Preziosi, D. Josephl and M. Arney, *J. Colloid Interface Sci.*, 1988, **124**, 552–559.
- 30 P. Petitjeans and T. Maxworthy, *J. Fluid Mech.*, 1996, **326**, 37–56.
- 31 C.-Y. Chen and E. Meiburg, *J. Fluid Mech.*, 1996, **326**, 57–90.
- 32 X. Cheng, L. Xu, A. Patterson, H. M. Jaeger and S. R. Nagel, *Nat. Phys.*, 2008, **4**, 234–237.
- 33 J. Nittman, G. Daccord and M. Stanley, *Nature*, 1985, **314**, 391.
- 34 S.-Y. Lee, E. Bettelheim and P. Wiegmann, *Phys. D*, 2006, **219**, 22–34.